


Meniscus osculation and adsorption on geometrically structured wallsMartin Pospíšil *Department of Physical Chemistry, University of Chemical Technology, Prague, 166 28 Praha 6, Czech Republic
and Department of Molecular Modelling, Institute of Chemical Process Fundamentals,
Czech Academy of Sciences, 165 02 Prague, Czech Republic*

Andrew O. Parry

*Department of Mathematics, Imperial College London, London SW7 2BZ, United Kingdom*Alexandr Malijevský *Department of Physical Chemistry, University of Chemical Technology, Prague, 166 28 Praha 6, Czech Republic
and Department of Molecular Modelling, Institute of Chemical Process Fundamentals,
Czech Academy of Sciences, 165 02 Prague, Czech Republic*

(Received 15 February 2022; accepted 18 May 2022; published 2 June 2022)

We study the adsorption of simple fluids at smoothly structured, completely wet walls and show that a meniscus osculation transition occurs when the Laplace and geometrical radii of curvature of locally parabolic regions coincide. Macroscopically, the osculation transition is of fractional, $\frac{7}{2}$, order and separates regimes in which the adsorption is microscopic, containing only a thin wetting layer, and mesoscopic, in which a meniscus exists. We develop a scaling theory for the rounding of the transition due to thin wetting layers and derive critical exponent relations that determine how the interfacial height scales with the geometrical radius of curvature. Connection with the general geometric construction proposed by Rascón and Parry is made. Our predictions are supported by a microscopic model density functional theory for drying at a sinusoidally shaped hard wall where we confirm the order of the transition and also an exact sum rule for the generalized contact theorem due to Upton. We show that as bulk coexistence is approached the adsorption isotherm separates into three regimes: A preosculation regime where it is microscopic, containing only a thin wetting layer; a mesoscopic regime, in which a meniscus sits within the troughs; and finally another microscopic regime where the liquid-gas interface unbinds from the crests of the substrate.

DOI: [10.1103/PhysRevE.105.064801](https://doi.org/10.1103/PhysRevE.105.064801)**I. INTRODUCTION**

Capillary condensation [1–7], wetting [8–13], and wedge filling [14–22] are but a few examples of surface phase transitions in which the surface tension plays a crucial role determining the location of the phase boundary and even the nature of the transition itself. Recent studies of capillary condensation in open slits, possessing corners or edges, have also highlighted another phase transition involving the depinning of the meniscus, located at the end(s) of the capillary as the pressure is increased [23,24]. At a macroscopic level, meniscus depinning is continuous with the order of the transition depending on the wetting properties of the confining walls. For example, it is third order if the walls are completely wet and second order if they are partially wet. In each case, the transition is rounded or smoothed by a mesoscopic length scale, specifically the parallel correlation length, associated with wetting layers at the capillary walls. The crossover scaling describing the rounding of meniscus depinning shows a remarkable consistency with the underlying theory of wetting transitions, including conjectured critical exponent relations, giving physically intuitive results for mesoscopic corrections

to macroscopic predictions for the adsorption at the phase boundary.

In this paper we point out that there is another type of phase transition involving a meniscus in a different confining geometry, which can be understood macroscopically, which is also rounded by mesoscopic wetting length scales. We refer to this as meniscus osculation and is associated with the vanishing of the meniscus, that is, the change from macroscopic to microscopic adsorption, when its curvature coincides with the geometrical curvature of a confining sculpted wall that is completely wet. As we will show, macroscopically, meniscus osculation is continuous but of fractional order, different from depinning, and that the rounding, while also due to wetting behavior, is described by a different crossover scaling theory. This crossover scaling will allow us to make a connection with very general expectations of how substrate geometry influences wetting behavior.

Our paper is arranged as follows. In Sec. II we recall briefly the macroscopic and crossover scaling theory for meniscus depinning, emphasizing the underlying consistency with the theory of (complete) wetting. We then turn to meniscus osculation, beginning first with the macroscopic description before

discussing the rounding due to complete wetting layers. This allows us to make a connection with a more general proposal for how geometry influences adsorption on structured surfaces [25]. In Secs. III and IV we present the results of a microscopic model density functional theory (DFT) study of adsorption at a corrugated sinusoidal wall, which shows not only meniscus osculation but also a modified complete wetting transition. Indeed, as the chemical potential approaches bulk coexistence, we show that the adsorption changes from being determined by microscopic length scales (preosculation) to macroscopic (geometry-dominated) length scales and back to microscopic length scales when it eventually unbinds from the crests of the sinusoid.

II. MENISCUS DEPINNING AND MENISCUS OSCULATION

Before describing the osculation transition, we recall the macroscopic and mesoscopic crossover scaling theory for meniscus depinning in an open capillary, following closely the presentation in Refs. [23,24]. This will act as a guide for developing and interpreting the scaling theory for the osculation transition occurring in parabolic and sinusoidally corrugated geometries.

A. Meniscus depinning

1. Macroscopic

Consider an open capillary, made from two opposing planar walls separated by a distance L . The bottom wall is of infinite extent while the top wall is of finite length H , which for our present purposes we suppose is much larger than L . Each end of the capillary is a right-angle edge and is in contact with a bulk reservoir of gas at temperature T , far below the bulk critical temperature T_c , and pressure p (or chemical potential μ) below bulk saturation p_{sat} (see Fig. 1). We define $\delta p = p_{\text{sat}} - p$. All the walls are considered completely wet by the liquid phase corresponding to an equilibrium contact angle $\theta = 0$. We suppose that the pressure is sufficiently close to bulk saturation that the fluid within the capillary has already condensed to a liquidlike phase. For very long capillaries, this capillary condensation will occur near $\delta p_{\text{CC}} \approx 2\gamma/L$, as dictated by the macroscopic Kelvin equation, where γ is the surface tension of the liquid-gas interface. The full H dependence of the pressure shift δp_{CC} can be determined but is not needed for the present purposes [23,24]. The capillary liquid phase is characterized by two menisci, each of which is an arc of circles of Laplace radius $R = \gamma/\delta p$ located near the ends of the capillary. Since the equilibrium contact angle $\theta = 0$, these meet the bottom wall tangentially. However, there are two possibilities for how they attach to the top wall. For $\delta p > \delta p_{\text{MD}}$, with $\delta p_{\text{MD}} = \gamma/L$, the menisci are pinned at the corners and are characterized by an edge contact angle θ_e . This is pressure dependent, given by

$$\theta_e = \cos^{-1} \left(\frac{L - R}{R} \right). \quad (1)$$

As the pressure is increased, the edge contact angle increases until at $\delta p = \delta p_{\text{MD}}$, equivalent to $R = L$, it reaches its maximum value $\theta_e = \pi/2$, at which point it is tangential to the

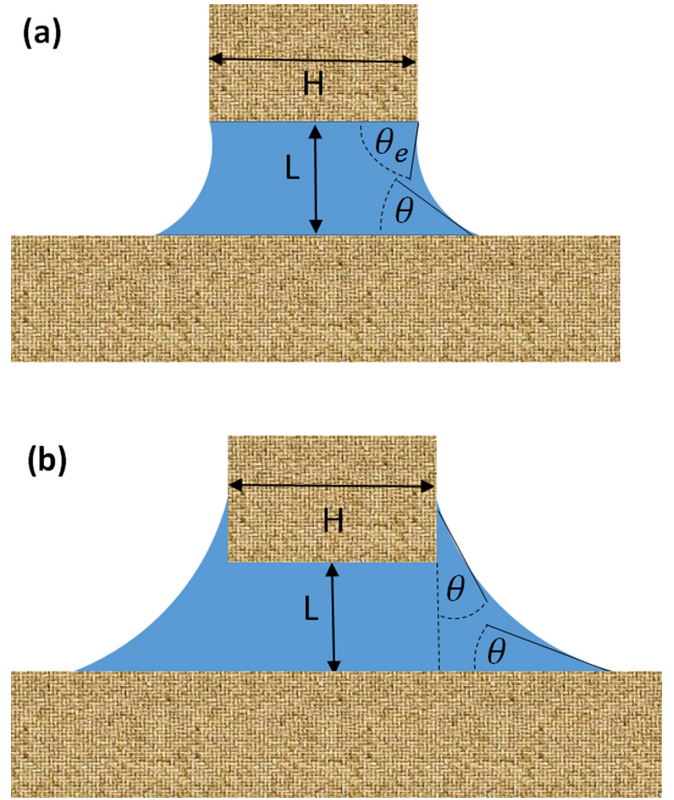


FIG. 1. Schematic illustration of two possible condensed capillary liquid phases in an open slit. (a) The two circular menisci of the Laplace radius of curvature are pinned at the upper edges, which they meet at an edge contact angle θ_e . The bottom of the menisci meets the horizontal lower wall at the equilibrium contact angle θ . (b) The two circular menisci are unpinned, spilling out into the right-angle corners and meet both the vertical and lower walls at the contact angle θ .

vertical sides of the upper wall and hence the menisci are no longer pinned. Clearly, at the point of this depinning the menisci are each a quarter circle which just fits inside the open ends of the capillary. For $\delta p < \delta p_{\text{MD}}$ the menisci are unpinned and meet the side walls tangentially at a distance $R - L$ above the corners. For complete wetting, meniscus depinning is a continuous third-order phase transition. This is most easily seen by determining the excess adsorption $\Delta\Gamma$ beyond the contribution $\Delta\rho HL$ from the volume of liquid within the capillary, with $\Delta\rho$ the difference in the bulk liquid and gas densities. For the pinned phase, with $R < L$, this is given by

$$\Gamma = 2\Delta\rho R^2 \left[\sin\theta_e + \frac{\sin 2\theta_e}{4} + \frac{1}{2}(\theta_e - \pi) \right], \quad (2)$$

while in the unpinned phase, for which $R > L$, it is given trivially by

$$\Gamma = 2\Delta\rho \left(1 - \frac{\pi}{4} \right) R^2. \quad (3)$$

It is then easy to check that the second derivative of the adsorption is discontinuous at the depinning transition

satisfying

$$\frac{\partial^2 \Gamma}{\partial R^2} = \begin{cases} \Delta\rho(4 - \pi), & \delta p = \delta p_{\text{MD}}^- \\ \Delta\rho(2 - \pi), & \delta p = \delta p_{\text{MD}}^+ \end{cases} \quad (4)$$

This is associated with a discontinuity in the third derivative of the grand potential (per unit length of the capillary), showing that the transition is indeed third order at the present macroscopic level.

2. Mesoscopic

The third-order meniscus depinning transition is rounded by length scales associated with complete wetting layers which coat the bottom and side walls. The mechanism for this rounding is different from the standard finite-size-scaling theory of the rounding of phase transitions when the available volume is finite (or the dimensionality is below that of the lower critical dimension), which is due to fluctuations [26,27]. The rounding of the meniscus depinning transition is not due to fluctuation effects but rather due to mesoscopic length scales which smooth the transition from pinned to unpinned states. Meniscus depinning is not associated with coexisting phases, symmetry breaking, or a diverging order parameter and therefore there cannot be any true critical behavior. The rounding of this transition is present as soon as we go beyond the macroscopic level, for example, in mean-field DFT or even simpler interfacial models which accommodate the presence of wetting layers. The length scales of relevance here are the wetting layer thickness $\ell_\pi \sim \delta p^{-\beta_s^{\text{co}}}$ and parallel correlation length $\xi_{\parallel} \sim \delta p^{-\nu_{\parallel}^{\text{co}}}$, arising from interfacial fluctuations, which characterize wetting layers at planar walls, close to bulk saturation. We note that the critical exponents depend on the range of the intermolecular forces, but always satisfy the exact exponent relation [8–13]

$$1 + \beta_s^{\text{co}} = 2\nu_{\parallel}^{\text{co}}, \quad (5)$$

which is of relevance to the crossover scaling theory for the rounding of the meniscus depinning transition. This exponent relation is the consequence of an exact sum rule which determines that for wetting transitions $\partial\Gamma/\partial\mu \propto \xi_{\parallel}^2$ [28]. As described above, macroscopically, the depinning transition occurs when $R = L$. Certainly, we can anticipate that the presence of the wetting layer at the bottom wall decreases the effective width of the slit by ℓ_π . However, of greater relevance is the rounding arising from the parallel correlation ξ_{\parallel} , associated with the wetting layer at the vertical side walls, which smooths the point of contact of the upper part of the meniscus with the corner (see Fig. 2). Since ξ_{\parallel} is larger than ℓ_π we can therefore expect that the depinning begins to occur when

$$R - L \approx \xi_{\parallel}. \quad (6)$$

This simple finite-size-scaling observation is the basis for the crossover theory. The purely macroscopic result (4) implies that the grand potential contains a singular contribution $\Omega_{\text{sing}} = \gamma(R - L)^3/6L^2$. To allow for the rounding due to complete wetting layers, we modify this by a multiplicative scaling function $W_{\text{MD}}(x)$ whose argument is the dimensionless scaling variable $x = (R - L)/\xi_{\parallel}$. Thus, the appropriate scaling

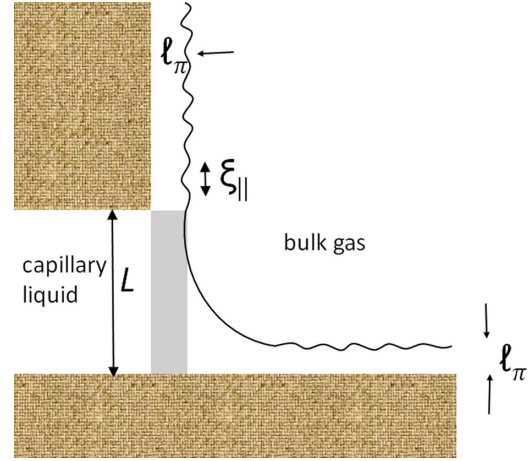


FIG. 2. Schematic illustration of the length scales determining the mesoscopic rounding of the continuous meniscus depinning transition, due to wetting layers adsorbed along the bottom and side walls. The macroscopic phase boundary $R = L$ for meniscus depinning is rounded by the wetting layer thickness ℓ_π and parallel correlation length ξ_{\parallel} along the bottom and top walls, respectively. The gray area depicts an additional contribution to the excess adsorption $\Gamma \propto \ell_\pi L$ due to the presence of the wetting layers.

ansatz is

$$\Omega_{\text{sing}} = \frac{(R - L)^3}{L^2} W_{\text{MD}}\left(\frac{R - L}{L\nu_{\parallel}^{\text{co}}}\right), \quad (7)$$

where we have ignored all constants and metric factors and substituted that, near the depinning transition, the correlation length scales with the slit width as $\xi_{\parallel} \approx L\nu_{\parallel}^{\text{co}}$. We require that $W_{\text{MD}}(x) \rightarrow 0$ as $x \rightarrow \infty$ and $W(x) \rightarrow 1$ as $x \rightarrow -\infty$, which represent the macroscopic unpinned and pinned states, respectively. The form of $W_{\text{MD}}(x)$ describes the smooth crossover between these two states when the mesoscopic wetting length scale ξ_{\parallel} is allowed for. In order that Ω_{sing} is nonzero at the macroscopic meniscus depinning transition $R = L$, we require that $W_{\text{MD}}(x) \propto 1/x^3$, which leads to a singular or mesoscopic contribution. The derivative of Ω_{sing} with respect to δp determines the singular contribution to the adsorption, over and above the macroscopic contribution $\Gamma \propto L^2$. Since $\partial\Omega/\partial\delta p \propto R^2\partial\Omega/\partial R$ it follows that the adsorption contains a singular contribution

$$\Gamma_{\text{sing}} = (R - L)^2 \Lambda_{\text{MD}}\left(\frac{R - L}{L\nu_{\parallel}^{\text{co}}}\right), \quad (8)$$

where $\Lambda_{\text{MD}}(x)$ is a suitable new scaling function. We require that $\Lambda_{\text{MD}}(x) \rightarrow 0$ as $x \rightarrow \infty$, $\Lambda_{\text{MD}}(x) \rightarrow 1$ as $x \rightarrow -\infty$, and $\Lambda_{\text{MD}}(x) \propto 1/x^2$ as $x \rightarrow 0$. It follows that exactly at the (macroscopic) depinning phase boundary $R = L$, the excess adsorption contains a mesoscopic contribution $\Gamma_{\text{sing}} \propto L^{2\nu_{\parallel}^{\text{co}}}$ in addition to the leading-order macroscopic term $\Gamma = 2\Delta\rho(1 - \frac{\pi}{4})L^2$ determined earlier. Using the exact exponent relation (5), it follows that the mesoscopic term can be written

$$\Gamma_{\text{sing}} \propto \ell_\pi L, \quad R = L, \quad (9)$$

which is of course simply the additional contribution to the adsorption from the meniscus when we shift its position by the thickness of a wetting layer $\ell_\pi \sim L^{\beta_s^{\text{co}}}$ coating the side walls

(see Fig. 2). Explicitly, for systems with dispersion forces this yields $\Gamma_{\text{sing}} \propto L^{4/3}$.

Before moving on to consider the meniscus osculation transition we point out that the above crossover scaling theory has a remarkable internal consistency which appears to connect, very naturally, the macroscopic physics of the meniscus with the microscopic physics associated with wetting behavior. Suppose, for example, we did not know what length scale was responsible for rounding the depinning transition. Instead, we simply marry the macroscopic result that $\Gamma \approx (R - L)^2$ with the direct geometrical requirement that at $R = L$ there must be a higher-order contribution $L\ell_\pi$, due to the wetting layers at the side walls which just shift the position of the meniscus. To do this, we write $\Gamma_{\text{sing}} = (R - L)^2 \Lambda_{\text{MD}}[(R - L)/\lambda_{\text{MD}}]$, which contains an as yet undetermined length scale λ_{MD} responsible for the rounding. At $R = L$ it follows that the singular contribution must scale as λ_{MD}^2 , which we identify with $L\ell_\pi$. Substituting that $\ell_\pi \sim \delta p^{-\beta_s^{\text{co}}}$ and that $R = \gamma/\delta p$, it follows that the length scale responsible for the rounding must behave as $\lambda_{\text{MD}} \sim \delta p^{-(1+\beta_s^{\text{co}})/2}$. Using the exact exponent relation (5), it follows that length scale responsible for the rounding must be

$$\lambda_{\text{MD}} = \xi_{\parallel}, \quad (10)$$

consistent with Eq. (6). This is a remarkable self-consistency: Adding a geometrical shift to the adsorption, due to the wetting layer thickness ℓ_π , we have generated a length scale, associated with wetting, which is the parallel correlation length. In other words, crossover scaling demands that the exponent relation $1 + \beta_s^{\text{co}} = 2\nu_{\parallel}^{\text{co}}$ is true.

B. Osculation transition

1. Macroscopic

We now turn attention to the phenomenon of meniscus osculation and suppose that the confining wall has a cross section of a parabola

$$\psi(x) = \frac{x^2}{2R_w}, \quad (11)$$

with translational invariance assumed in the other direction. We restrict ourselves entirely to walls that are completely wet corresponding to equilibrium contact angle $\theta = 0$. The wall is again supposed to be in contact with a bulk gas at subcritical temperature T and pressure $p < p_{\text{sat}}$. As the pressure is increased to bulk coexistence the adsorption diverges due to the growth of a meniscus near the bottom of the parabola. At a macroscopic level this once again takes the shape of a circular arc of Laplace radius $R = \gamma/\delta p$ which meets the walls tangentially at $\pm x_0$ at height z_0 . We denote by ℓ_0 the height of the meniscus above the bottom (see Fig. 3). These length scales are trivially determined, yielding

$$x_0 = \sqrt{R^2 - R_w^2}, \quad (12)$$

$$z_0 = \frac{R^2 - R_w^2}{2R_w}, \quad (13)$$

$$\ell_0 = \frac{(R - R_w)^2}{2R_w}. \quad (14)$$

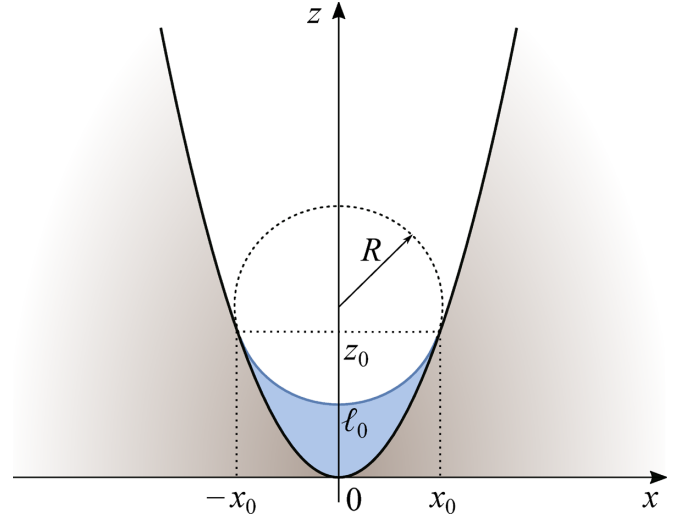


FIG. 3. Geometrical construction determining the macroscopic meniscus of a parabolic, completely wet wall. The dashed circle is of $R = \gamma/\delta p$ and connects with the wall tangentially at points $(-x_0, z_0)$ and (x_0, z_0) . The height of the meniscus above the wall is ℓ_0 . The construction is only possible if R is larger than the geometrical radius of curvature at the bottom R_w .

As pointed out in Ref. [25], as $\delta p \rightarrow 0$ these length scales diverge with universal exponents which are geometry dominated, independently of the range of the intermolecular forces. More generally, for walls which have a power-law cross section $\psi(x) \propto |x|^\phi$, the divergence of the adsorption as $\delta p \rightarrow 0$ is geometry dominated provided $\phi > \beta_s^{\text{co}}/\nu_{\parallel}^{\text{co}}$. For $\phi < \beta_s^{\text{co}}/\nu_{\parallel}^{\text{co}}$ the adsorption diverges similarly to complete wetting at a planar wall which depends strongly on the range of intermolecular forces. Returning to the parabola, we focus here on the *disappearance* of the meniscus as the pressure is reduced to point at which

$$R = R_w. \quad (15)$$

We refer to this as meniscus osculation. Macroscopically, for $R < R_w$ there is no adsorption of liquid at the walls since no meniscus can be fitted into the geometry. More generally, beyond the macroscopic level, meniscus osculation separates regimes in which the adsorption is geometry dominated and microscopic, respectively. Associated with the osculation is a singular contribution to the grand potential Ω per unit length of the wall. At a purely macroscopic level this is determined by

$$\Omega = \delta p A + \gamma(\ell_m - \ell_w), \quad (16)$$

where A is the area of liquid, ℓ_m is the meniscus length, and ℓ_w is the contact length of the liquid with the wall. Again, these are very simply determined as

$$A = \frac{x_0}{3R_w}(2R^2 + R_w^2) - R^2 \sin^{-1}\left(\frac{x_0}{R}\right), \quad (17)$$

$$\ell_m = R \sin^{-1}\left(\frac{\sqrt{R^2 - R_w^2}}{R}\right), \quad (18)$$

and

$$\ell_w = \frac{R}{R_w} \sqrt{R^2 - R_w^2} + R_w \sinh^{-1} \left(\frac{\sqrt{R^2 - R_w^2}}{R_w} \right). \quad (19)$$

This implies that the grand potential is given explicitly by

$$\frac{\Omega}{\gamma} = \frac{\sqrt{R^2 - R_w^2}}{3R_w} \left(\frac{R_w^2}{R} - R \right) + R \sin^{-1} \left(\frac{\sqrt{R^2 - R_w^2}}{R} \right) - R_w \sinh^{-1} \left(\frac{\sqrt{R^2 - R_w^2}}{R_w} \right). \quad (20)$$

As the pressure is decreased and R reduces to R_w , this exhibits the (macroscopic) critical singularity

$$\frac{\Omega}{\gamma} \approx -\frac{16\sqrt{2}}{105} \frac{(R - R_w)^{7/2}}{R_w^{5/2}}, \quad (21)$$

which is of fractional higher order than the third-order meniscus depinning. The derivative of the grand potential determines the associated singularity in the adsorption, which disappears as

$$\Gamma_{\text{sing}} \approx \frac{8\sqrt{2}}{15} \frac{\Delta\rho(R - R_w)^{5/2}}{\sqrt{R_w}}, \quad (22)$$

which is simply $\Delta\rho$ times the meniscus area A . For $R < R_w$ there is no macroscopic adsorption.

Meniscus osculation is closely related to the phenomenon of capillary emptying in horizontal capillaries, under the influence of gravity, of an elliptical cross section [29]. Specifically, the rich phase behavior associated with emptying is related to whether menisci, which now represent the cross-sectional shape of horizontal liquid tongues, can be locally inscribed within the ellipse (see, e.g., the cross sections shown in Figs. 1 and 2 in Ref. [29]).

2. Mesoscopic

Similar to depinning, the continuous osculation transition must be rounded by length scales due to mesoscopic complete wetting layers. There will always be some residual microscopic adsorption even when $R < R_w$, implying that the crossover from the geometry-dominated regime $R > R_w$ must be smooth since there is neither symmetry breaking nor any diverging order parameter or length scale. For the meniscus depinning the rounding of the macroscopic phase boundary $R = L$ can be understood directly, by considering how the macroscopic meniscus attaches to the edge of the opening when wetting layers are present, leading to $R - L \approx \xi_{\parallel}$. This line of reasoning is not so obvious for the rounding at osculation since the meniscus itself is disappearing. The simplest length scale and observable to focus on is the value of the interfacial height ℓ_0 when $R = R_w$, for which there is no macroscopic contribution. We wish to determine how, exactly at osculation $R = R_w$, the interfacial height scales with the radius of curvature and introduce a new osculation critical exponent β_{osc} to characterize this,

$$\ell_0 \approx R_w^{\beta_{\text{osc}}}, \quad R = R_w, \quad (23)$$

where we have omitted any unimportant dimensional prefactors. To determine the osculation exponent, we suppose that in

the vicinity of the osculation transition the interfacial height shows crossover scaling

$$\ell_0 = \frac{(R - R_w)^2}{2R_w} \mathcal{L}_{\text{osc}} \left(\frac{R - R_w}{\lambda_{\text{osc}}} \right), \quad (24)$$

with λ_{osc} the undetermined rounding length scale and $\mathcal{L}_{\text{osc}}(x)$ the appropriate scaling function. The macroscopic limit, corresponding to Eq. (14), is recovered by imposing that $\mathcal{L}_{\text{osc}}(x) \rightarrow 1$ as $x \rightarrow \infty$. We also require that $\mathcal{L}_{\text{osc}}(x) \sim x^{-2}$ as $x \rightarrow 0$, in order that at osculation the value of ℓ_0 remains finite, implying $\ell_0 \propto \lambda_{\text{osc}}^2/R_w$. Since the wall is completely wet we also require that this diverges as $R_w \rightarrow \infty$, i.e., as we follow the line of osculation transitions to bulk coexistence. This means that we can eliminate the possibility that the rounding length scale is the planar wetting layer thickness ℓ_{π} , since in that case ℓ_0 does not diverge. In addition, the identification $\lambda_{\text{osc}} \approx \xi_{\parallel}$, while appropriate for meniscus depinning, is unsatisfactory since, on using the exact exponent relation (5), this only yields $\ell_0 \approx \ell_{\pi}$. This is most likely only a lower bound since it is physically reasonable that the residual interfacial height at osculation is greater than the planar wetting layer thickness at the same pressure.

To identify the rounding length scale we instead focus on the value of ℓ_0 deep in the preosculation regime $R_w \gg R$ and ensure that our scaling ansatz is compatible with the necessary curvature-induced enhancement of the adsorption. For wetting on spheres and cylinders of radius R_c , say, which have a negative curvature, it is well known that the increase in the surface tension contribution thins the wetting layer equivalent to a shift in the effective value of the partial pressure from δp to $\delta p + \gamma/R_c$ [30–34]. For the parabola it is therefore reasonable to expect that when $R_w \gg R$ the local interface height is enhanced by the positive curvature so that ℓ_0 is the same as the planar wetting layer thickness but evaluated at an effective reduced partial pressure $\delta p - \gamma/R_w$, i.e., $\ell_0 \rightarrow (1/R - 1/R_w)^{-\beta_s^{\text{co}}}$. This requirement is highly restrictive and is only compatible with the crossover scaling ansatz (24) provided that the scaling function $\mathcal{L}_{\text{osc}}(x) \propto |x|^{-2-\beta_s^{\text{co}}}$ as $x \rightarrow -\infty$ and identifies that the rounding length-scale scales with R_w and R according to

$$\lambda_{\text{osc}}^{2+\beta_s^{\text{co}}} = R_w^{1+\beta_s^{\text{co}}} R^{\beta_s^{\text{co}}}, \quad (25)$$

where again we have omitted unimportant microscopic length scales. Using this value for λ_{osc} , it follows that the osculation and wetting exponents are related via

$$\beta_{\text{osc}} = \frac{3\beta_s^{\text{co}}}{2 + \beta_s^{\text{co}}}, \quad (26)$$

which is the central prediction of our mesoscopic scaling theory. In three dimensions and with dispersion forces and also in two dimensions with short-range forces, for which $\beta_s^{\text{co}} = \frac{1}{3}$, this predicts that $\beta_{\text{osc}} = \frac{3}{7}$, pointing to a rather nontrivial interplay between geometry and wetting at osculation. In three dimensions and with short-range forces it is likely that the prediction $\beta_{\text{osc}} = 0$ corresponds to a logarithmic dependence of ℓ_0 on R_w . Having identified the rounding length scale λ_{osc} , the crossover scaling theory can be applied to other quantities. For example, we can expect that the singular contribution to

the grand potential per length scales as

$$\Omega = \frac{(R - R_w)^{7/2}}{R_w^{5/2}} W_{\text{osc}} \left(\frac{R - R_w}{\lambda_{\text{osc}}} \right), \quad (27)$$

where we have ignored the prefactors. The scaling function $W_{\text{osc}}(x)$ must satisfy $W_{\text{osc}}(\infty) = 1$ in order to recover the macroscopic singularity in the geometry-dominated regime. On approaching the osculation transition at $R = R_w$, the scaling function must also behave as $W_{\text{osc}} \propto x^{-7/2}$ in order to leave a finite singular contribution, which we define as

$$\Omega \approx R_w^{2-\alpha_{\text{osc}}}. \quad (28)$$

This identifies the exponent as

$$2 - \alpha_{\text{osc}} = \frac{3}{2} \left(\frac{3\beta_s^{\text{co}} - 1}{2 + \beta_s^{\text{co}}} \right), \quad (29)$$

again relating it to the singularities at complete wetting. This exponent relation is noteworthy because it predicts that $2 - \alpha_{\text{osc}} = 0$ when $\beta_s^{\text{co}} = \frac{1}{3}$, as is pertinent to three-dimensional systems with dispersion forces and two-dimensional systems with short-range forces, and is presumably indicative of a marginal logarithmic singularity. We mention this because precisely the same marginal singularity is predicted for meniscus depinning for systems with dispersion forces [23,24]. Exactly at the depinning transition $R = L$, the singular contribution to the grand potential is predicted to be $\Omega \approx L^{2-\alpha_{\text{MD}}}$, where $2 - \alpha_{\text{MD}} = (3\beta_s^{\text{co}} - 1)/2$, which obviously also vanishes when $\beta_s^{\text{co}} = \frac{1}{3}$. The vanishing of both these exponents is consistent with the known marginal logarithmic contribution to the free energy of a finite-size droplet in these systems [35]. This consistency between osculation, depinning, and complete wetting for systems with dispersion forces is not achieved if we choose $\lambda_{\text{osc}} \approx \xi_{\parallel}$ which, as mentioned above, we believe is a lower bound for the rounding length scale at osculation.

The prediction of the mesoscopic crossover scaling theory, which at osculation ℓ_{π} is a lower bound for the value of ℓ_0 , is consistent with a simple idea proposed by Rascón and Parry, who suggested that the total adsorption on a completely wet sculpted surface can be determined by first coating the wall with a wetting layer of thickness ℓ_{π} , defined normal to each surface point [25]. This coating modifies the original wall shape $\psi(x) \rightarrow \tilde{\psi}(x)$, onto which we then fit a meniscus of Laplace radius R . This simple modified macroscopic construction reproduces with remarkable accuracy different scaling regimes, arising due to the competition between microscopic forces and geometry, obtained from numerical studies of interfacial Hamiltonian models and experiments [36–38]. We will return to this in the next section.

III. ADSORPTION ON A CORRUGATED WALL

In preparation for studying meniscus osculation in a microscopic DFT, we turn our attention to the adsorption occurring near a sinusoidally corrugated wall described by the height function

$$\psi(x) = A \left[1 - \cos \left(\frac{2\pi x}{L} \right) \right], \quad (30)$$

where A is the amplitude and L is the period. The axes here are chosen such that $\psi = 0$ at the bottom wall. The adsorption and wetting properties on such corrugated surfaces have been studied previously, but usually concentrating on the partial wetting regime where, for simple fluids, prewetting and unbending transitions (equivalent to a local condensation of liquid within the troughs) compete [39–44]. The surface behavior is very rich for complex fluids (liquid crystals) where dislocations near the crests must be taken into account [45,46]. Here we restrict ourselves to simple fluids and to complete wetting ($\theta = 0$) where none of these features are present. In spite of this, the adsorption isotherm is still quite rich and we anticipate falls into three regimes (see Fig. 4).

A. Microscopic preosculation regime

When the pressure is low, such that the Laplace radius of curvature $R \ll R_w$, where $R_w = L^2/4\pi^2 A$, no meniscus is present. In this case the adsorption is entirely microscopic comprising a thin wetting layer of approximate thickness ℓ_{π} which coats the wall. As the pressure is increased, a rounded meniscus osculation transition occurs near $R = R_w - \lambda_{\text{osc}}$, where the adsorption changes from microscopic to macroscopic due to the growth of the meniscus. In three-dimensional systems and for short-range forces $\lambda_{\text{osc}} \approx \sqrt{R_w}$ and therefore is of a similar size to ξ_{\parallel} . A signature of this rounded transition would be a dramatic change in the behavior of the second and third derivatives $\partial^2 \Gamma / \partial \mu^2$ and $\partial^3 \Gamma / \partial \mu^3$, respectively, which reflect the fractional order of the macroscopic transition.

B. Macroscopic geometry-dominated regime

When $R < R_w$ a meniscus sits near the troughs of the corrugated wall connecting tangentially with its sides. As the pressure is increased the meniscus grows until it is near the crests of the sinusoid. Macroscopically, this geometry-dominated regime extends from osculation ($R = R_w$), equivalent to

$$\delta p_{\text{osc}} = \frac{4\pi^2 A \gamma}{L^2}, \quad (31)$$

to saturation, $\delta p = 0$. It can again be shown easily that for the sinusoidal wall (30) the height of the meniscus above the bottom is

$$\ell_0 = z_0 + \sqrt{R^2 - x_0^2} - R, \quad (32)$$

where $\pm x_0$ and z_0 are the coordinates denoting the contact of the meniscus with the wall (see Fig. 3) which are given implicitly by solving simultaneously

$$A \sin \left(\frac{2\pi x_0}{L} \right) = \frac{L x_0}{2\pi \sqrt{R^2 - x_0^2}} \quad (33)$$

and

$$z_0 = A \left[1 - \cos \left(\frac{2\pi x_0}{L} \right) \right]. \quad (34)$$

The presence of wetting layers qualitatively and quantitatively affects this and is described approximately by the Rascón-Parry (RP) construction, in which we coat the wall with the wetting layer prior to fitting inside the circular meniscus (see

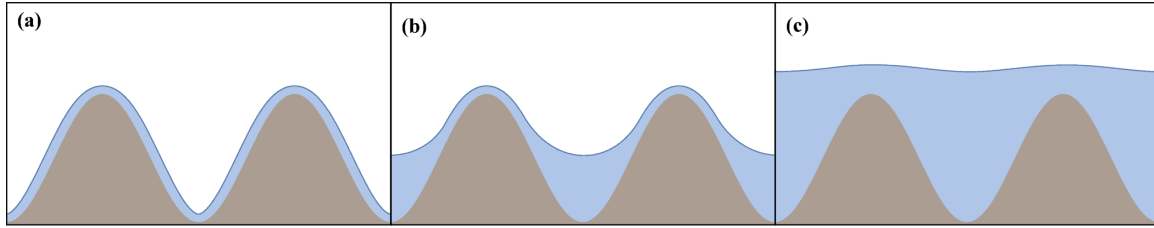


FIG. 4. Schematic illustration of three possible adsorption regimes of a completely wet ($\theta = 0$) sinusoidal wall. (a) In the low-adsorption preosculation regime, far away from bulk coexistence, a microscopic amount of liquid coats the wall and the liquid-gas interface follows the wall shape. (b) Within the second regime, the voids of the wall become gradually filled with liquid. (c) In the third regime, the liquid-gas interface unbinds from the wall and its height diverges as the coexistence is approached, similarly, but not identically, to planar walls. While the first and third regimes are governed by microscopic forces, the second regime is controlled by the wall geometry and can be described macroscopically.

Fig. 5). Similarly, the approach to saturation is more properly a crossover from a geometry-dominated regime where the meniscus lies within the wells to a second microscopic regime where the liquid-gas interface unbinds from the crests. This second crossover occurs when the period $L \approx \xi_{||}$, i.e., when the characteristic scale of the interfacial fluctuations is similar to the geometric scale.

C. Microscopic interfacial unbinding regime

On approaching saturation, the liquid-gas interface must unbind from the wall and will display properties which are very similar to complete wetting at a planar surface. The divergence of the film thickness in this limit cannot be described macroscopically and we must allow for the intermolecular forces and the effective binding that result between the interface and the wall. The shape of the wall does have some influence on the equilibrium shape of the liquid-gas interface, but this is negligible, at *leading order*, when the parallel correlation length is larger than the period L , corresponding to the regime $\delta p \ll L^{-1/\nu_{||}^{co}}$ in which case the interface is effectively planar. Critical exponents which characterize the divergence of the film thickness and parallel correlation length are unchanged. The question whether there is any signature of the wall shape on the complete wetting layer, as it unbinds from the crests, is rather subtle and is related to the nature of the binding potential. This is particularly subtle for systems with short-range forces and we intend to focus on this problem in a separate work [47].

IV. DFT ANALYSIS OF ADSORPTION ON A SINUSOIDAL HARD WALL

Here we present the results for adsorption on a sinusoidal hard wall obtained using a microscopic DFT. We present first the model whose accuracy we test using an exact sum rule due to Upton [48]. Numerical results illustrating the meniscus osculation transition and different adsorption regimes are then presented.

A. Density functional theory

Consider a simple fluid which is subject to an external field $V(\mathbf{r})$ due to a presence of a confining wall and which is in contact with a bulk reservoir at temperature T and chemical potential μ . Within classical DFT [49] the equilibrium density

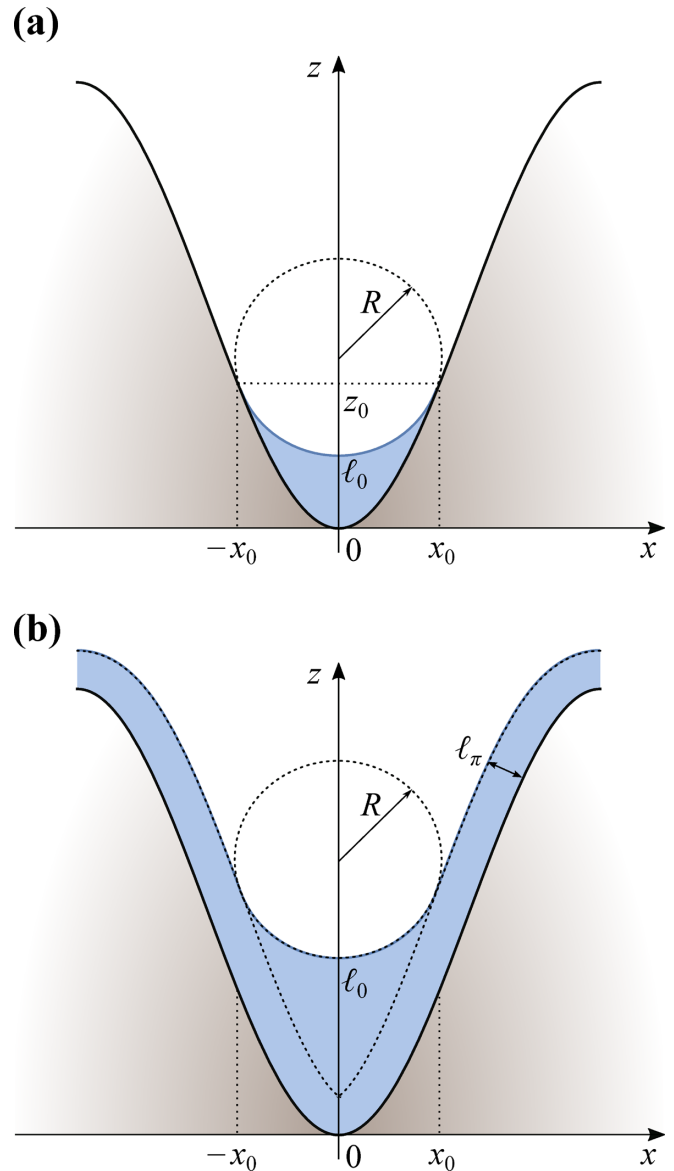


FIG. 5. Schematic illustration of (a) geometrical construction for macroscopic meniscus in a sinusoidal wall and (b) modified RP construction where the wall is first coated by a uniform layer of thickness ℓ_π .

profile $\rho(\mathbf{r})$ of the fluid is obtained by minimization of the grand potential functional

$$\Omega[\rho] = F[\rho] + \int d\mathbf{r} \rho(\mathbf{r})[V(\mathbf{r}) - \mu], \quad (35)$$

where $F[\rho]$ is the intrinsic free-energy functional containing all the information about the fluid interactions. Its approximation, which is a crucial part of any DFT model, depends largely on the choice of the fluid model and particularly for simple fluids the intrinsic free energy can be treated in a perturbative manner

$$F[\rho] = F_{\text{id}}[\rho] + F_{\text{HS}}[\rho] + F_{\text{att}}[\rho], \quad (36)$$

which splits the functional into the ideal gas F_{id} , repulsive hard-sphere F_{HS} , and attractive F_{att} contributions.

The ideal gas part is known exactly and is given by

$$\beta F_{\text{id}}[\rho] = \int d\mathbf{r} \rho(\mathbf{r}) \{\ln[\rho(\mathbf{r})\Lambda^3] - 1\}, \quad (37)$$

where Λ is the thermal de Broglie wavelength which can be set to unity and $\beta = 1/k_B T$ is the inverse temperature.

The repulsive interaction between fluid molecules is approximated by the hard-sphere potential and its contribution to the free energy is described accurately using Rosenfeld's fundamental measure theory [50]

$$F_{\text{HS}}[\rho] = \frac{1}{\beta} \int d\mathbf{r} \Phi(\{n_\alpha\}), \quad (38)$$

where $\{n_\alpha\}$ denotes a set of six weighted densities

$$n_\alpha(\mathbf{r}) = \int d\mathbf{r}' \rho(\mathbf{r}') \omega_\alpha(\mathbf{r} - \mathbf{r}'), \quad \alpha = \{0, 1, 2, 3, v1, v2\}, \quad (39)$$

given by convolutions between the one-body fluid density $\rho(\mathbf{r})$ and the weight functions $\{\omega_\alpha\}$ which characterize so-called fundamental measures of the hard-sphere particles of diameter σ :

$$\omega_3(\mathbf{r}) = \Theta(\mathcal{R} - |\mathbf{r}|), \quad \omega_2(\mathbf{r}) = \delta(\mathcal{R} - |\mathbf{r}|), \quad (40)$$

$$\omega_1(\mathbf{r}) = \frac{\omega_2(\mathbf{r})}{4\pi\mathcal{R}}, \quad \omega_0(\mathbf{r}) = \frac{\omega_2(\mathbf{r})}{4\pi\mathcal{R}^2}, \quad (41)$$

$$\omega_{v2}(\mathbf{r}) = \frac{\mathbf{r}}{\mathcal{R}} \delta(\mathcal{R} - |\mathbf{r}|), \quad \omega_{v1}(\mathbf{r}) = \frac{\omega_{v2}(\mathbf{r})}{4\pi\mathcal{R}}. \quad (42)$$

Here Θ is the Heaviside function, δ is Dirac's delta function, and $\mathcal{R} = \sigma/2$. Among various possible prescriptions for describing the free-energy density Φ for inhomogeneous hard-sphere fluid, we adopt the original Rosenfeld approximation [50], which accurately describes short-range correlations between fluid particles and satisfies exact statistical mechanical sum rules [6].

For separations $r > \sigma$, a pair of fluid particles is assumed to interact via the attractive part of the Lennard-Jones potential $u_{\text{att}}(r)$, which is truncated at a cutoff which we set to be $r_c = 2.5\sigma$, i.e.,

$$u_{\text{att}}(r) = \begin{cases} 0, & r < \sigma \\ -4\varepsilon\left(\frac{\sigma}{r}\right)^6, & \sigma < r < r_c \\ 0, & r > r_c. \end{cases} \quad (43)$$

This attractive contribution is modeled in simple mean-field fashion

$$F_{\text{att}}[\rho] = \frac{1}{2} \iint d\mathbf{r} d\mathbf{r}' \rho(\mathbf{r}) \rho(\mathbf{r}') u_{\text{att}}(|\mathbf{r} - \mathbf{r}'|). \quad (44)$$

We assume that the external potential is a hard wall of sinusoidal shape

$$V(x, z) = \begin{cases} \infty, & z < \psi(x) \\ 0, & z > \psi(x), \end{cases} \quad (45)$$

where $\psi(x)$ is given by Eq. (30). A purely hard wall is known to be completely dry, i.e., completely wet by vapor, corresponding to contact angle $\theta = \pi$. By studying drying we are also able to avoid the complications arising from layering since liquid layers are absent near the surface of the wall. We assume that the wall is of a macroscopic extent in the remaining Cartesian direction and the system is thus translationally invariant along the y axis.

The minimization of (35) leads to the self-consistent equation for the equilibrium density profile

$$\rho(\mathbf{r}) = \Lambda^{-3} \exp[\beta\mu - \beta V(\mathbf{r}) + c^{(1)}(\mathbf{r})], \quad (46)$$

where $c^{(1)}(\mathbf{r}) = c_{\text{HS}}^{(1)}(\mathbf{r}) + c_{\text{att}}^{(1)}(\mathbf{r})$ is the one-body direct correlation function, which can be split into the hard-sphere contribution

$$c_{\text{HS}}^{(1)}(\mathbf{r}) = - \sum_{\alpha} \int d\mathbf{r}' \frac{\partial \Phi(\{n_\alpha\})}{\partial n_\alpha} \omega_\alpha(\mathbf{r}' - \mathbf{r}) \quad (47)$$

and the attractive part

$$c_{\text{att}}^{(1)}(\mathbf{r}) = -\beta \int d\mathbf{r}' u_{\text{att}}(|\mathbf{r} - \mathbf{r}'|) \rho(\mathbf{r}'). \quad (48)$$

We solve Eq. (46) numerically on a rectangular discrete grid of spacing of 0.1σ using Picard iteration where the convolutions in (39), (47), and (48) are determined using a fast Fourier transform [51].

From the equilibrium density profile $\rho(x, z)$ we can extract the local height of the liquid-gas interface identified as

$$\rho(x, \ell(x)) = \frac{\rho_g + \rho_l}{2} \quad (49)$$

and also the excess adsorption

$$\Gamma = \int_{-L/2}^{L/2} dx \int_{\psi(x)}^{\infty} dz [\rho_b - \rho(x, z)], \quad (50)$$

where ρ_b is the bulk density. In our numerical study, we are of course not able to model a semi-infinite system; instead, we set the density equal to the bulk density at a fixed distance of 50σ above the crests of the sinusoid.

B. DFT results

1. Upton sum rule

The contact sum rule for a planar hard wall in contact with a bulk fluid (i.e., in a semi-infinite geometry) elegantly relates the fluid density at contact ρ_w to the bulk pressure [6]:

$$\beta p = \rho_w. \quad (51)$$

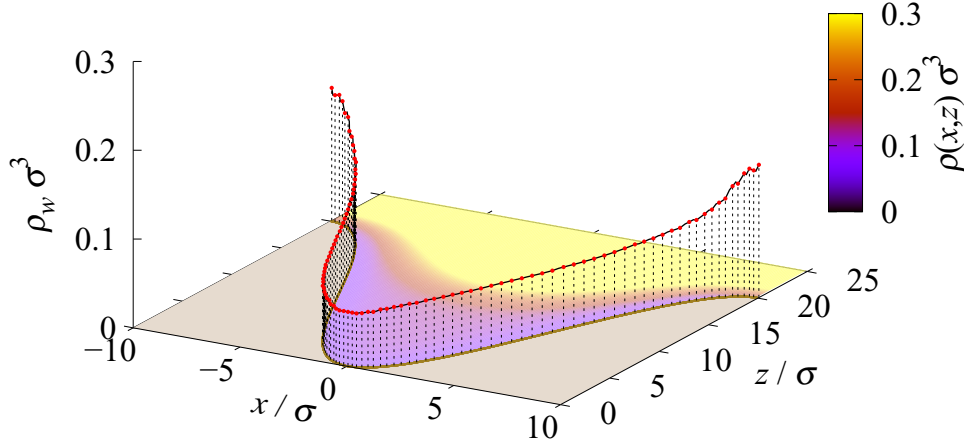


FIG. 6. Three-dimensional plot of the contact density profile for a corrugated hard wall (30) over a single period with $L = 20\sigma$ and $A = 10\sigma$, which is in contact with a supersaturated bulk liquid at $\delta\mu = 0.0023\varepsilon$. The black line with red dots represents the value of the local contact density $\rho(\mathbf{s})$, where $\mathbf{s} = (x, \psi(x))$. The corresponding full DFT density profile, in the form of a colormap on the xz plane, is also shown.

For nonplanar hard walls, the contact density becomes position dependent and the theorem generalizes to [48]

$$\beta p = \bar{\rho}_w. \quad (52)$$

Here $\bar{\rho}_w$ is the geometrically averaged contact density defined as

$$\bar{\rho}_w = \frac{1}{A_w} \int \rho(\mathbf{s}) ds, \quad (53)$$

where the integration is over the wall surface of total area $A_w = \int ds$. Here $\rho(\mathbf{s})$ is the value of the contact density at position x , with $\mathbf{s} = (x, \psi(x))$, and $ds = dx\sqrt{1 + \psi'(x)^2}$ is the local area element.

Being exact, the contact theorem is a useful test of the accuracy of the numerical methods used to solve Eq. (46). Errors arise in a number of ways, including the discretization used in the Picard iteration and also from finite-size effects, since we have to impose that the density takes its bulk value at some finite distance (which we set to be 50σ) above the crests. In Fig. 6 we plot the numerically determined contact density along the corrugated wall, from which we can determine the geometrically averaged contact density $\beta p / \bar{\rho}_w$. As anticipated, the local density is smallest at the troughs and highest at the crests. In Fig. 7 we plot the numerically determined value of $\beta p / \bar{\rho}_w$ as a function of the chemical potential for two different wall amplitudes and periods which we use to study the meniscus osculation transition and adsorption isotherms. For the shallower geometry, with $L = 100\sigma$ and $A = 20\sigma$, there is very good agreement with the prediction of the Upton sum rule with the worst relative error about 2%. For the more corrugated wall with $L = 30\sigma$ and $A = 30\sigma$ the agreement is still good but a little worse with the maximum relative error about 7%.

2. Osculation transition and meniscus shapes

We now turn our attention to the adsorption occurring on sinusoidal walls for a range of periodicities and amplitudes. All the DFT calculations were performed at a temperature

$T = 0.925T_c$, where T_c is the critical temperature of the bulk fluid ($k_B T_c = 1.41\varepsilon$). At this temperature, the corresponding densities of the coexisting bulk gas and liquid phases are $\rho_g = 0.104\sigma^{-3}$ and $\rho_l = 0.431\sigma^{-3}$, respectively, and the chemical potential of saturation is $\mu_{\text{sat}} = -3.943\varepsilon$.

At least qualitatively, the equilibrium density profile $\rho(x, z)$ and adsorption fall into the three regimes as described earlier. This is illustrated in Fig. 8 for the more corrugated wall where $L = 30\sigma$ and $A = 30\sigma$. In the density profile we also highlight the local height of the liquid-gas interface $\ell(x)$, which is shown as the green line. Of particular interest is the local height above the wall bottom ℓ_0 , whose dependence on

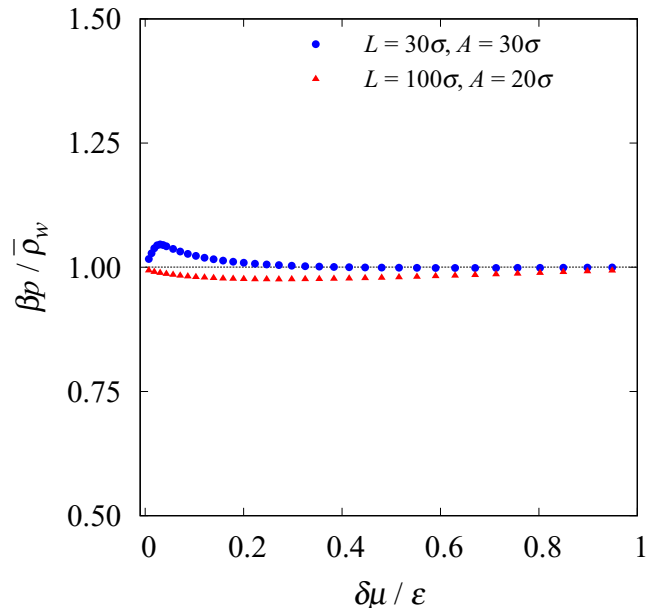


FIG. 7. Numerical DFT results for the dimensionless ratio $\beta p / \bar{\rho}_w$ as a function of the bulk fluid supersaturation $\delta\mu$ for two different wall amplitudes and periods showing good agreement with Upton's generalized contact theorem (52).

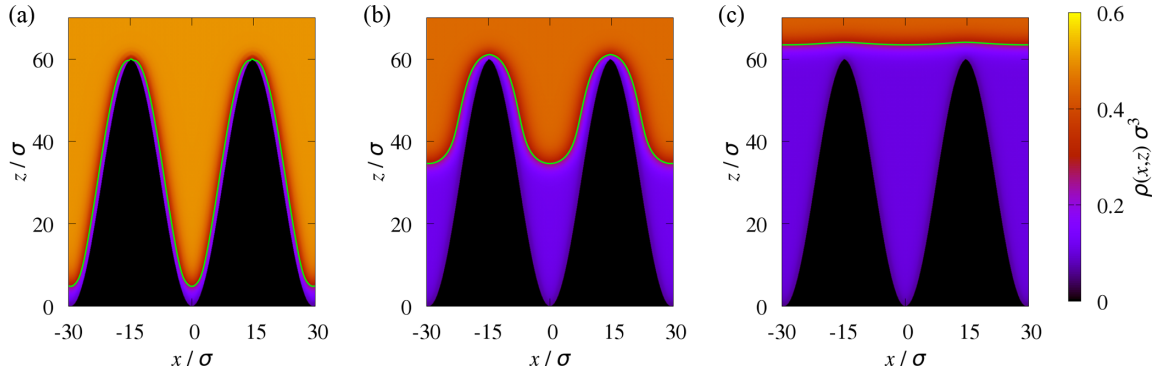


FIG. 8. Numerical DFT results for the equilibrium density profiles for the sinusoidal hard wall with $L = 30\sigma$ and $A = 30\sigma$ illustrating (a) a microscopic preosculation regime, (b) a macroscopic geometry-dominated regime, and (c) a microscopic interface unbinding regime, which correspond to the three points highlighted in Fig. 9. The green line denotes the equilibrium height $\ell(x)$ of the liquid-gas interface.

the chemical potential is shown in Fig. 9. Figures 8(a)–(c) and the corresponding points on the adsorption of Fig. 9 correspond to (i) the microscopic preosculation regime, (ii) the macroscopic geometry-dominated regime, and (iii) the microscopic interfacial unbinding regime, respectively.

Now we seek to be more quantitative. Numerical evidence for a (rounded) osculation transition is shown in Fig. 10 for the shallower geometry with $L = 100\sigma$ and $A = 20\sigma$, where we plot the second and third derivatives of the excess adsorption as a function of μ . The corresponding growth of the midpoint height ℓ_0 is shown in Fig. 11 together with state points whose profiles we will compare with the predictions of the geometric construction. It can be seen from Fig. 10 that in contrast to the second derivative $\partial^2\Gamma/\partial\mu^2$, the third derivative $\partial^3\Gamma/\partial\mu^3$ undergoes a dramatic increase near $\delta\mu/\varepsilon \approx 0.01$. This qualitative difference between the second and third derivatives is consistent with the macroscopic $\frac{5}{2}$ singularity

predicted for the osculation transition [recall Eq. (22)]. The sudden increase in the third derivative occurs close to the value of the chemical potential where the meniscus lifts off the trough [see Figs. 12(c) and 12(d)]. Next we focus on the geometry-dominated regime and test the macroscopic and mesoscopic predictions of Sec. III B for the shape and height of the meniscus. In Fig. 11 we compare the growth of the meniscus height ℓ_0 with the macroscopic prediction (32) and its mesoscopic correction following the RP construction. The purely macroscopic prediction is only in semiquantitative agreement with the DFT results. The predicted height ℓ_0 is systematically lower than the DFT results, which suggests that the discrepancy is mainly due to the presence of thin drying layers which are allowed for, approximately, in the RP construction. The accuracy of this construction for the

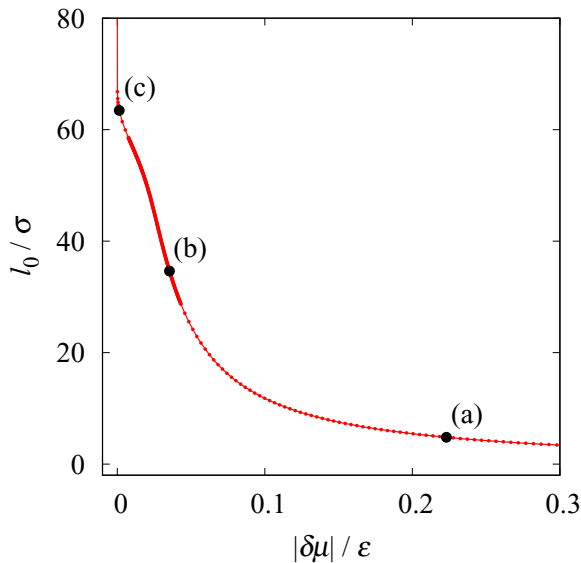


FIG. 9. Growth of the height of the liquid-gas interface ℓ_0 measured above the wall bottom, for the sinusoidal hard wall with $L = 30\sigma$ and $A = 30\sigma$. The points (a), (b), and (c) correspond to the density profiles shown in Fig. 8 representative of the three adsorption regimes.

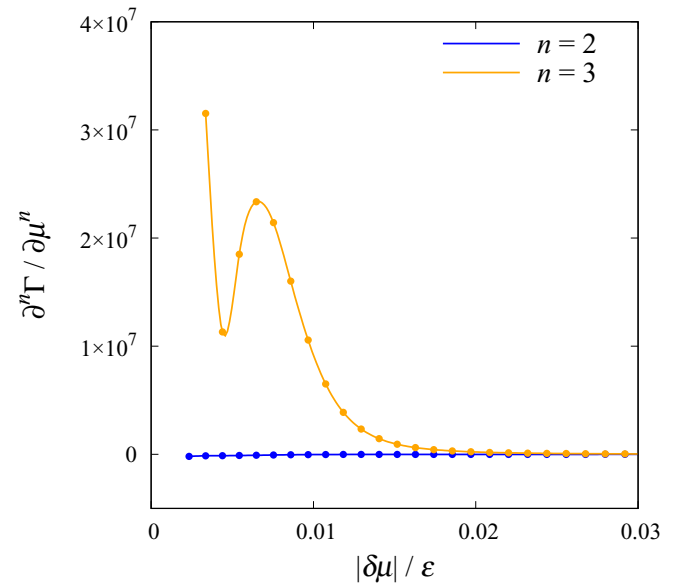


FIG. 10. Numerical DFT results comparing the second (blue line) and third (orange line) derivatives of the excess adsorption Γ with respect to μ for a sinusoidal hard wall with $L = 100\sigma$ and $A = 20\sigma$. The dramatic increase in the third derivative near $\delta\mu/\varepsilon \approx 0.01$ closely coincides with the growth of a meniscus near the bottom of the wall corresponding to a rounded meniscus transition.

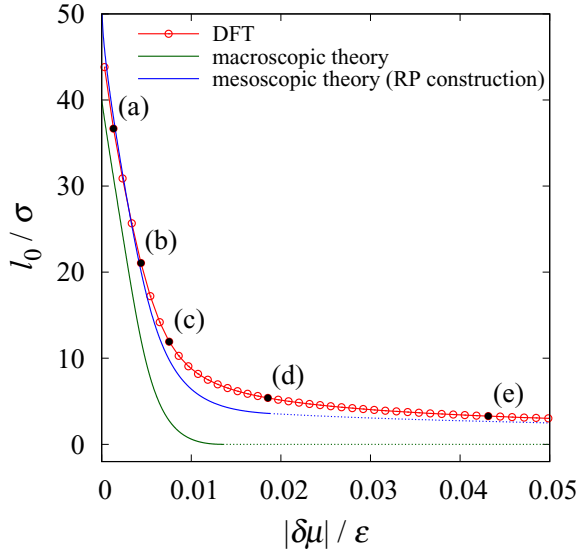


FIG. 11. Comparison of the numerical DFT results (red symbols) for ℓ_0 as a function of $\delta\mu$ with the predictions of the purely macroscopic theory (green line) and RP mesoscopic construction (blue line) for a sinusoidal hard wall with $L = 100\sigma$ and $A = 20\sigma$. The continuation of the green and blue lines beyond the osculation transition are denoted by the respective dotted lines.

meniscus shape is illustrated in Fig. 12 for five representative DFT density profiles corresponding to the thermodynamic points highlighted in Fig. 11. In these figures we can compare the true shape of the interfacial profile $\ell(x)$ (green solid line) with the prediction of the RP construction (green dashed line). The RP construction gives significantly better agreement with the DFT results (see the blue line in Fig. 11). The RP construction is particularly accurate for the state points (a) and (b) where the meniscus is higher up the trough, meeting the wall above the points of inflection of the sinusoid. It is probably not coincidental that the comparison between the DFT results and the prediction of the RP construction is worst near the osculation transition. In these plots we have also highlighted a green circle of Laplace radius R which we have purposely placed to touch the *true* value of ℓ_0 . It is apparent that the interfacial shape $\ell(x)$ is always well described by the arc of the circular meniscus in the central region of the trough. However, it is clear from these plots that the simple RP scheme of first coating the wall with the uniform layer of ℓ_π slightly overestimates the adsorption at the crests and slightly underestimates the true interfacial height above the troughs. It might be possible to modify the RP construction by allowing for some local geometric dependence on the wetting that we first coat the wall with before inserting the arc of the circular Laplace meniscus.

Further comparisons between the purely macroscopic and the RP predictions with the DFT results are presented in Fig. 13 for various wall parameters. In Figs. 13(a)–13(c) we vary the wall amplitude for the fixed periodicity ($L = 100\sigma$), while in Figs. 13(d)–13(f) the periodicity is varied for the fixed amplitude ($A = 20\sigma$). In general, the agreement between the mesoscopic theory and the DFT is close but somewhat deteriorates as the ratio A/L increases. This is most likely

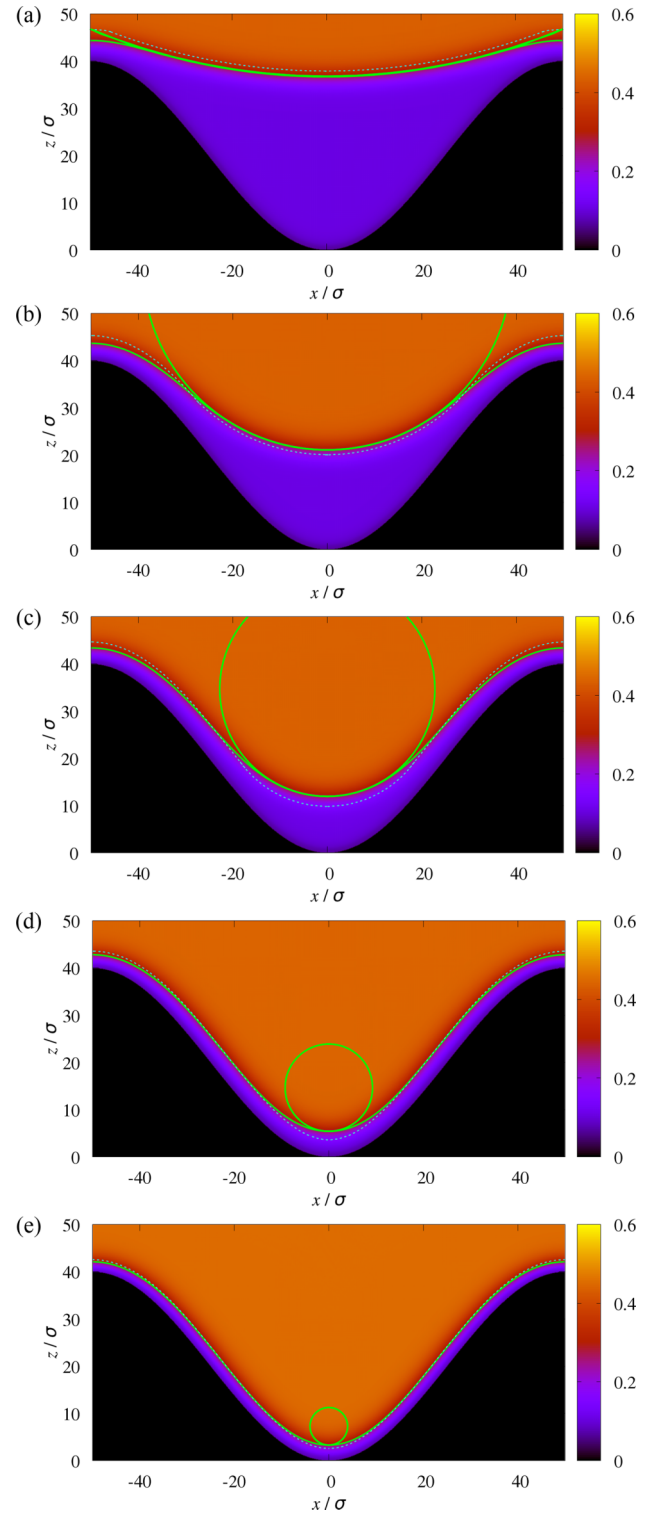


FIG. 12. Equilibrium DFT density profiles, $\rho(x, z)\sigma^3$, over a single period for the sinusoidal hard wall with the periodicity $L = 100\sigma$ and amplitude $A = 20\sigma$ corresponding to the points in Fig. 11. For each of these profiles, three curves are highlighted. The green solid curve is the DFT result for the location of the interface $\ell(x)$, defined as the locus where the local fluid density is $(\rho_g + \rho_l)/2$. This is compared with two other curves. The green solid circle has the Laplace radius R and has been placed so that its lowest point coincides with the true value of ℓ_0 . The green dashed line is the RP prediction for $\ell(x)$.

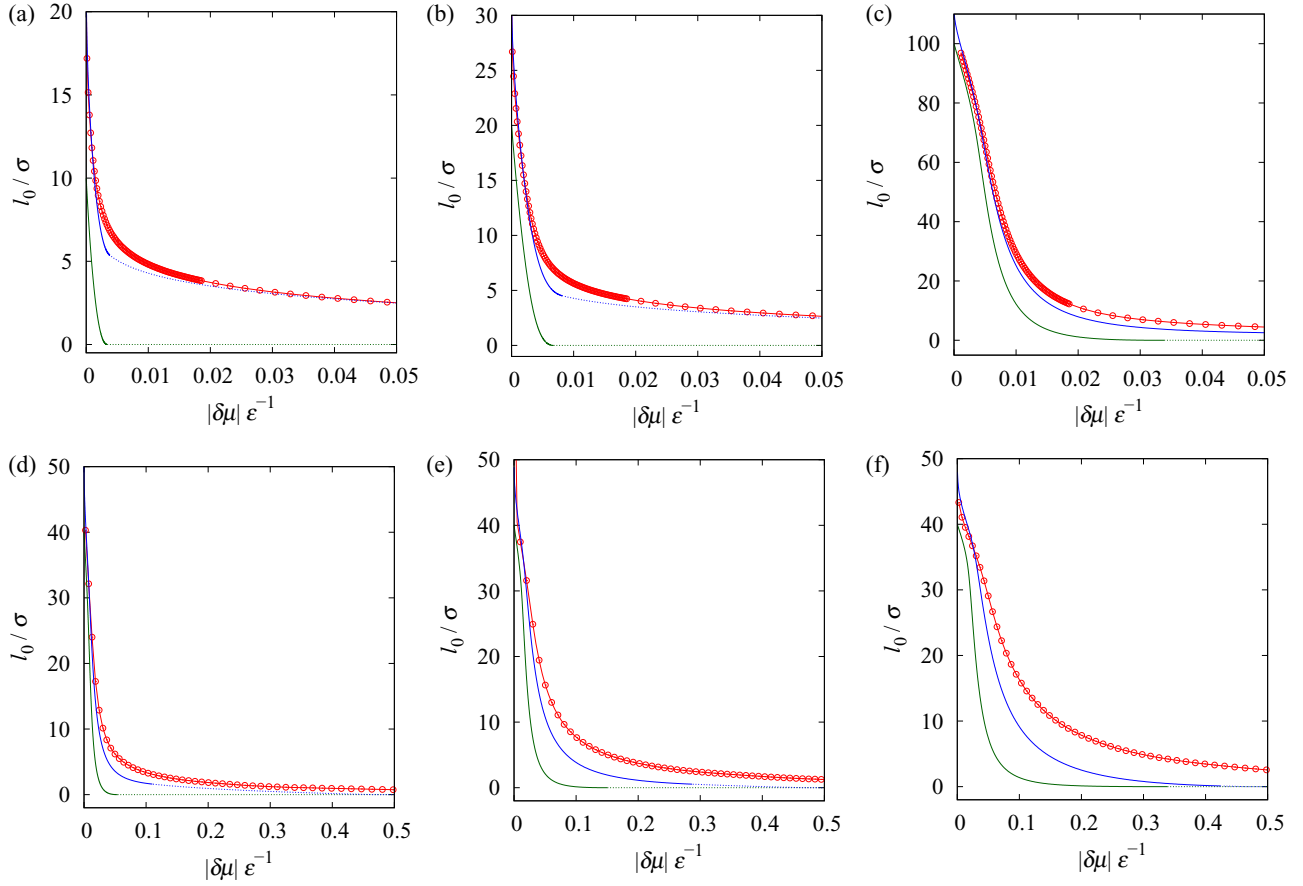


FIG. 13. (a)–(c) Comparison of the meniscus height ℓ_0 as a function of $\delta\mu$ obtained from DFT (red symbols), the macroscopic theory (green line), and the mesoscopic RP construction (green line) for a sinusoidal hard wall with the fixed periodicity $L = 100\sigma$ and varying amplitude: (a) $A = 5\sigma$, (b) $A = 10\sigma$, and (c) $A = 50\sigma$. (d)–(f) Same comparison as in (a)–(c) but for a hard sinusoidal wall of fixed amplitude $A = 20\sigma$ and varying periodicity: (d) $L = 50\sigma$, (e) $L = 30\sigma$, and (f) $L = 20\sigma$. Note that the scale of the abscissa in (d)–(f) is an order of magnitude larger than in (a)–(c).

because for highly curved walls any small discrepancy in ℓ_π or R has a significant impact on the resulting value of ℓ_0 . It appears that for sinusoidal walls the condition $A = L$ represents the limit beyond which even the mesoscopic RP construction ceases to be quantitatively reliable.

V. SUMMARY

In this paper we have studied the adsorption of fluids at smoothly corrugated completely wet walls using macroscopic theory, mesoscopic scaling theory, and microscopic DFT. In particular, we have focused on a rounded meniscus osculation transition occurring near the trough of the sinusoid which is associated with the appearance of a meniscus as the chemical potential is increased towards bulk saturation. Macroscopically, this transition is of $\frac{7}{2}$ order but is rounded due to the influence of a thin wetting layer arising from microscopic interactions. The scaling theory that we developed for this predicts a nontrivial relationship between the interfacial height at the osculation and the wetting layer thickness. The simple RP construction for mesoscopic corrections within the geometry-dominated regime was tested in our DFT where we showed that it accurately describes the adsorption on the corrugated surface, particularly where the meniscus is above the points

of inflection of the wall. For a sinusoidal wall the adsorption falls into three regimes: the preosculation regime, where the adsorption is determined by the microscopic interactions; a postosculation regime, where the meniscus sits within the troughs of the wall; and finally a complete wetting regime, where the interface unbinds from the crests. This final regime can again be only understood by taking into account the microscopic interactions. Our work can be extended in many ways. In particular, it will be necessary to test the prediction for the value of the osculation exponent $\beta_{\text{osc}} = \frac{3}{7}$ in systems with dispersion forces and also in two dimensions. Also, recall that for meniscus depinning the order of the phase transition changes when the walls are partially wet. This may also occur for meniscus osculation where the phase transition also competes with wetting and unbending transitions [39]. The surface phase diagram may be very rich in these systems, similar to predictions for wetting on chemically patterned surfaces. Returning to the case of complete wetting, our DFT results suggest that one may modify and improve the RP construction by allowing curvature corrections to the thin wetting layer that first coats the wall. Finally, it would be interesting to examine in more detail how the shape of the wall influences the divergence of the adsorption due to the unbinding of the liquid-gas interface as bulk coexistence is approached. To

correctly understand this, it is necessary to model the effect of interaction between the interface and the wall using the fully nonlocal binding potential [52].

ACKNOWLEDGMENTS

This work was financially supported by the Czech Science Foundation Project No. 20-14547S.

-
- [1] M. E. Fisher and H. Nakanishi, *J. Chem. Phys.* **75**, 5857 (1981).
- [2] H. Nakanishi and M. E. Fisher, *J. Chem. Phys.* **78**, 3279 (1983).
- [3] R. Evans and P. Tarazona, *Phys. Rev. Lett.* **52**, 557 (1984).
- [4] R. Evans and U. Marini Bettolo Marconi, *Chem. Phys. Lett.* **114**, 415 (1985).
- [5] R. Evans, P. Tarazona, and U. Marini Bettolo Marconi, *J. Chem. Phys.* **84**, 2376 (1986).
- [6] *Fundamentals of Inhomogeneous Fluids*, edited by D. Henderson (Dekker, New York, 1992).
- [7] L. D. Gelb, K. E. Gubbins, R. Radhakrishnan, and M. Sliwiska-Bartkowiak, *Rep. Prog. Phys.* **62**, 1573 (1999).
- [8] D. E. Sullivan and M. M. Telo da Gama, in *Fluid Interfacial Phenomena*, edited by C. A. Croxton (Wiley, New York, 1986).
- [9] S. Dietrich, in *Phase Transitions and Critical Phenomena*, edited by C. Domb and J. L. Lebowitz (Academic, New York, 1988), Vol. 12.
- [10] J. S. Rowlinson and B. Widom, *Molecular Theory of Capillarity* (Clarendon, Oxford, 1989).
- [11] M. Schick, in *Liquids and Interfaces*, edited by J. Chorvolin, J. F. Joanny, and J. Zinn-Justin (Elsevier, New York, 1990).
- [12] G. Forgacs, R. Lipowsky, and T. M. Nieuwenhuizen, in *Phase Transitions and Critical Phenomena*, edited by C. Domb and J. L. Lebowitz (Academic, London, 1991), Vol. 14.
- [13] D. Bonn, J. Eggers, J. Indekeu, J. Meunier, and E. Rolley, *Rev. Mod. Phys.* **81**, 739 (2009).
- [14] E. H. Hauge, *Phys. Rev. A* **46**, 4994 (1992).
- [15] K. Rejmer, S. Dietrich, and M. Napiórkowski, *Phys. Rev. E* **60**, 4027 (1999).
- [16] A. O. Parry, C. Rascón, and A. J. Wood, *Phys. Rev. Lett.* **83**, 5535 (1999).
- [17] D. B. Abraham and A. Maciołek, *Phys. Rev. Lett.* **89**, 286101 (2002).
- [18] G. Delfino and A. Squarcini, *Phys. Rev. Lett.* **113**, 066101 (2014).
- [19] A. Milchev, M. Müller, K. Binder, and D. P. Landau, *Phys. Rev. Lett.* **90**, 136101 (2003); *Phys. Rev. E* **68**, 031601 (2003).
- [20] N. R. Bernardino, A. O. Parry, and J. M. Romero-Enrique, *J. Phys.: Condens. Matter* **24**, 182202 (2012).
- [21] A. Malijevský and A. O. Parry, *Phys. Rev. Lett.* **110**, 166101 (2013).
- [22] A. Malijevský and A. O. Parry, *J. Phys.: Condens. Matter* **25**, 305005 (2013).
- [23] A. Malijevský and A. O. Parry, *Phys. Rev. Lett.* **127**, 115703 (2021).
- [24] A. Malijevský and A. O. Parry, *Phys. Rev. E* **104**, 044801 (2021).
- [25] C. Rascón and A. O. Parry, *Nature (London)* **407**, 986 (2000).
- [26] M. N. Barber, in *Phase Transitions and Critical Phenomena*, edited by C. Domb and J. L. Lebowitz (Academic, London, 1983), Vol. 8.
- [27] V. Privman and M. E. Fisher, *Phys. Rev. B* **30**, 322 (1984).
- [28] R. Evans and P. Tarazona, *Phys. Rev. Lett.* **53**, 400 (1984).
- [29] C. Rascón, A. O. Parry, and D. G. A. L. Aarts, *Proc. Natl. Acad. Sci. USA* **113**, 12633 (2016).
- [30] R. Hołyst and A. Poniewierski, *Phys. Rev. B* **36**, 5628 (1987).
- [31] T. Bieker and S. Dietrich, *Physica A* **252**, 85 (1998).
- [32] M. C. Stewart and R. Evans, *Phys. Rev. E* **71**, 011602 (2005).
- [33] A. O. Parry, C. Rascón, and L. Morgan, *J. Chem. Phys.* **124**, 151101 (2006).
- [34] A. Nold, A. Malijevský, and S. Kalliadasis, *Phys. Rev. E* **84**, 021603 (2011).
- [35] A. Malijevský, A. O. Parry, and M. Pospíšil, *Phys. Rev. E* **96**, 032801 (2017).
- [36] L. Bruschi, A. Carlin, and G. Mistura, *Phys. Rev. Lett.* **89**, 166101 (2002).
- [37] O. Gang, K. J. Alvine, M. Fukuto, P. S. Pershan, C. T. Black, and B. M. Ocko, *Phys. Rev. Lett.* **95**, 217801 (2005).
- [38] C. Rascón, *Phys. Rev. Lett.* **98**, 199801 (2007).
- [39] C. Rascón and A. O. Parry, *J. Phys.: Condens. Matter* **12**, A369 (2000).
- [40] K. Rejmer and M. Napiórkowski, *Phys. Rev. E* **62**, 588 (2000).
- [41] G. P. Kubalski, M. Napiórkowski, and K. Rejmer, *J. Phys.: Condens. Matter* **13**, 4727 (2001).
- [42] K. Rejmer, *Phys. Rev. E* **65**, 061606 (2002).
- [43] K. Rejmer, *Physica A* **373**, 58 (2007).
- [44] Á. Rodríguez-Rivas, J. Galván, and J. M. Romero-Enrique, *J. Phys.: Condens. Matter* **27**, 035101 (2015).
- [45] P. Patrício, N. M. Silvestre, C. T. Pham, and J. M. Romero-Enrique, *Phys. Rev. E* **84**, 021701 (2011).
- [46] P. Patrício, J. M. Romero-Enrique, N. M. Silvestre, N. R. Bernardino, and M. M. Telo da Gama, *Mol. Phys.* **109**, 1067 (2011).
- [47] M. Pospíšil, A. O. Parry, and A. Malijevský (unpublished).
- [48] P. J. Upton, *Phys. Rev. Lett.* **81**, 2300 (1998).
- [49] R. Evans, *Adv. Phys.* **28**, 143 (1979).
- [50] Y. Rosenfeld, *Phys. Rev. Lett.* **63**, 980 (1989).
- [51] A. G. Salinger and L. J. D. Frink, *J. Chem. Phys.* **118**, 7457 (2003).
- [52] A. O. Parry, C. Rascón, N. R. Bernardino, and J. M. Romero-Enrique, *J. Phys.: Condens. Matter* **18**, 6433 (2006).